

# Validation of the HZETRN Code for Laboratory Exposures with 1A GeV Iron Ions in Several Targets

S. A. Walker<sup>a</sup>, J. Tweed<sup>a</sup>, J. W. Wilson<sup>b</sup>, F. A. Cucinotta<sup>c</sup>, R. K. Tripathi<sup>b</sup>, S. Blattnig<sup>b</sup>, C. Zeitlin<sup>d</sup>, L. Heilbronn<sup>d</sup>, and J. Miller<sup>d</sup>

<sup>a</sup> *Old Dominion University, Norfolk, VA 23529 USA*

<sup>b</sup> *NASA Langley Research Center, Hampton, VA 23681-2199 USA*

<sup>c</sup> *NASA Johnson Space Center, Houston, TX 77058 USA*

<sup>d</sup> *Lawrence Berkeley National Laboratory, Berkeley, CA 94720 USA*

## Abstract

A new version of the HZETRN code capable of validation with HZE ions in either the laboratory or the space environment is under development. The computational model consists of the lowest order asymptotic approximation followed by a Neumann series expansion with non-perturbative corrections. The physical description includes energy loss with straggling, nuclear attenuation, nuclear fragmentation with energy dispersion and downshift. Measurements to test the model were performed at the Alternating Gradient Synchrotron and the NASA Space Radiation Laboratory at Brookhaven National Laboratory with iron ions. Surviving beam particles and produced fragments were measured with solid state detectors. Beam analysis software has been written to relate the computational results to the measured energy loss spectra of the incident ions for rapid validation of modeled target transmission functions.

## 1. Introduction

During a space mission, spacecraft are exposed to radiations of various types over a broad energy spectrum depending on location in space and time. Among the more important of these are heavy-ion cosmic radiations that originate from the sun and galactic sources. The shielding and exposure of crewmembers are controlled by the transport properties of these radiations through the spacecraft, its onboard systems and the bodies of the individuals themselves. Transport codes therefore play an important role in estimating and managing the radiation risk to the astronauts and their equipment. One way of reducing the radiation dose experienced is by the addition of shielding at those places within the spacecraft where large amounts of time are spent. In consequence, there is considerable interest in the development of new shielding materials. Since it is clearly impractical to verify the shielding properties of every candidate material and configuration in space, shield designers rely heavily upon models of radiation transport and measurements taken at particle accelerators, which play an important role in the model design and validation process.

Numerical solution methods for the Boltzmann transport equation are best suited to space radiations where the energy spectra are smooth over large energy intervals and less suited to the simulation of laboratory beams which exhibit large spectral variation over a very limited energy domain and large energy derivative. As a result, codes for space based on these numerical methods are not readily validated by comparison with laboratory experiment (Wilson et al. 1990). Only analytical procedures are able to simulate both space radiations and laboratory beam transport with equal ability in a common procedure and to that end a new version of the HZETRN code is currently under development. The computational model consists of combinations of physical perturbation expansions based on the scales of atomic interaction, multiple scattering, and nuclear reactive processes with use of Neumann-asymptotic expansions with non-perturbative corrections. The code contains energy loss with straggling, nuclear attenuation, nuclear fragmentation with energy dispersion and downshifts, and off-axis dispersion with multiple scattering under preparation. An asymptotic expansion has been used to simplify the transport of high charge and energy ions for broad beam applications in the laboratory and space. The solution of the lowest order asymptotic term is then related to a Green's function for energy loss and straggling coupled to nuclear attenuation providing the lowest order term in a rapidly converging Neumann series for which higher order collision terms are related to the fragmentation events including energy dispersion and downshift. Accurate analytic approximations have been obtained for the first two Neumann corrections and the Neumann series remainder estimated via a nonperturbative technique. Measurements to test the model were performed at the Alternating Gradient Synchrotron and the NASA Space Radiation Laboratory at Brookhaven National Laboratory using iron ions. Surviving beam particles and produced fragments were measured with solid-state detectors. Beam analysis software has been written to relate the computational results for the measured energy loss spectra of the incident ions and their fragments for rapid validation of modeled target material transmission functions.

## 2. The Transport Model

The types and energy distributions of particles transmitted through a shield material require the solution to the Boltzmann transport equation with appropriate boundary conditions related to the external radiation environment. With target fragments neglected, the first order asymptotic approximation to the transport equation takes the form (Wilson 1977)

$$\partial_x \phi_j(x, E) = \sum_{k \geq j} \int \sigma_{jk}(E, E') \phi_k(x, E') dE' - \sigma_j(E) \phi_j(x, E), \quad (1)$$

where  $\sigma_j(E)$  and  $\sigma_{jk}(E, E')$  are the media macroscopic cross sections. The  $\sigma_{jk}(E, E')$  represent all those processes by which type k particles moving in the x-direction with energy  $E'$  produce a type j particle with energy  $E$  moving in the same direction. Note that there may be several reactions that produce a particular product, and the appropriate cross sections for Eq. (1) are the inclusive ones. The total cross section  $\sigma_j(E)$  with the medium for each particle type of energy  $E$  may be expanded as  $\sigma_j(E) = \sigma_j^{at}(E) + \sigma_j^{el}(E) + \sigma_j^r(E)$ , where the first term refers to collision with atomic electrons, the second term is for elastic nuclear scattering, and the third term describes nuclear reactions. The corresponding differential cross section is given as

$$\sigma_{jk}(E, E') = \sum_n \sigma_{j,n}^{at}(E') \delta_{jk} \delta(E - E' + \varepsilon_n) + \sigma_j^{el}(E') \delta_{jk} \delta(E - E') + \frac{\sigma_{jk}^r(E')}{\sqrt{(2\pi)\varepsilon_{jk}(E')}} \exp\left[-\frac{(E + \lambda_{jk}(E') - E')^2}{2\varepsilon_{jk}(E')^2}\right], \quad (2)$$

where  $\varepsilon_n$  are the atomic/molecular excitation energy levels and where the collision energy downshift  $\lambda_{jk}(E')$  and corresponding energy width  $\varepsilon_{jk}(E')$  are approximated from the known momentum distributions observed in heavy ion reactions and represented by a Gaussian model (Tripathi et. al. 1994). Many atomic collisions ( $\sim 10^6$ ) occur in a centimeter of ordinary matter, whereas  $\sim 10^3$  nuclear coulomb elastic collisions occur per centimeter, while nuclear reactions are separated by a fraction to many centimeters depending on energy and particle type. This ordering allows flexibility in expanding solutions to the Boltzmann equation as a sequence of physical perturbative approximations.

In order to construct the solution we rewrite Eq. (1) in operator notation by defining the vector array field function  $\Phi = [\phi_j(x, E)]$ , the drift operator  $\mathbf{D} = [\partial_x]$  and the interaction operator

$\mathbf{I} = \Xi - \sigma = [\sum \int \sigma_{jk}(E, E') dE' - \sigma_j(E)]$ , with the understanding that  $\mathbf{I}$  has three parts associated with atomic, elastic, and reactive processes as given in Eq. (2). The transport equation is then written as

$$[\mathbf{D} - \mathbf{I}^{at} - \mathbf{I}^{el} + \sigma^r] \cdot \Phi = \Xi^r \cdot \Phi, \quad (3)$$

and hence may be expressed in the form

$$\Phi = [\mathbf{D} - \mathbf{I}^{at} - \mathbf{I}^{el} + \sigma^r]^{-1} \cdot \Phi_B + \int_{x'}^x [\mathbf{D} - \mathbf{I}^{at} - \mathbf{I}^{el} + \sigma^r]^{-1} \cdot \Xi^r \cdot \Phi dx_1 = \mathbf{G}^0 \cdot \Phi_B + \mathbf{Q} \cdot \mathbf{G}^0 \cdot \Xi^r \cdot \Phi, \quad (4)$$

where  $\Phi_B$  is the appropriate boundary condition and  $\mathbf{G}^0$  is the solution of the homogeneous form of Eq. (3) with a unit source at the boundary. Eq. (4) is a Volterra integral equation and (Wilson et. al. 1991) may be solved in a Neumann series as

$$\Phi = [\mathbf{G}^0 + \mathbf{Q} \cdot \mathbf{G}^0 \cdot \Xi^r \cdot \mathbf{G}^0 + \mathbf{Q} \cdot \mathbf{G}^0 \cdot \Xi^r \cdot \mathbf{Q} \cdot \mathbf{G}^0 \cdot \Xi^r \cdot \mathbf{G}^0 + \dots] \cdot \Phi_B = [\mathbf{G}^0 + \mathbf{G}^1 + \mathbf{G}^2 + \dots] \cdot \Phi_B, \quad (5)$$

with the elements of the leading term, the zero order Green's function, given as (Tweed et. al. 2004)

$$G_{jk}^0(x, x', E, E') = \frac{\delta_{jk}}{\sqrt{2\pi s_k(x-x', E')}} \frac{P_k[E']}{P_j[E]} \exp\left\{-\frac{[E - E_k(x-x', E')]^2}{2s_k(x-x', E')^2}\right\}, \quad (6)$$

where  $P_k(E) = \exp\left[-\int_0^E \frac{\sigma_k^r(E')}{\tilde{S}_k(E')} dE'\right]$  is the nuclear attenuation function,  $\tilde{S}_k(E)$  is the average change in  $E$  per unit path length per nucleon,  $R_k(E)$  is the usual range-energy relation,  $E_k(x-x', E) = R_k^{-1}[R_k(E) - (x-x')]$  is the mean energy for incident  $k$ -type particles of energy  $E'$  after a distance of penetration  $x-x'$  and  $s_k(x-x', E')$  is the corresponding rms deviation (Wilson et. al. 2002). Now that the propagator  $\mathbf{G}^0$  has been identified, the remaining terms in the Neumann series (5) may be found via the recurrence formula

$$\mathbf{G}^n = [\mathbf{Q} \cdot \mathbf{G}^0 \cdot \mathbf{\Xi}^r] \cdot \mathbf{G}^{n-1}, \quad n \geq 1. \quad (7)$$

The first Neumann correction  $\mathbf{G}^1$  is accurately evaluated over the saddle point whose width is determined by the energy dispersion and located at the downshifted ion collision specific energy. Introduction of the analytic first Neumann correction leads to significant simplification of the second correction term  $\mathbf{G}^2$ , allowing application of the mean value theorem and a similar second saddle point approximation. At sufficiently high energy, nuclear cross section variations are small and there is little variation in the normalized spectral shapes. Therefore, we can make use of a nonperturbative technique (Wilson et al., 1994a) to estimate the integral flux of the remaining terms and combine this with the normalized  $\mathbf{G}^2$  spectrum to approximate the Neumann series remainder.

### 3. The Detector Model

Solid state energy loss detectors, consisting of a layer of lithium-drifted silicon, are often used to estimate the charge and energy of particles in ion beam experiments. On passing through the detector, a charged particle liberates one electron-hole pair per 3.6 eV of energy deposited. The resulting signal is amplified, digitized, and stored for offline analysis. The direct measurement is therefore energy deposited in the detector.

Detectors of this type have a 'dead layer' which is estimated at  $3\% \pm 1.5\%$  of the total detector thickness. The charge liberated in this layer is lost, presumably to recombination, and therefore the energy released by the passing particle is slightly greater than the energy deposit measured. With high-energy beams, there are additional losses due to the production of high-energy delta electrons that escape the detector volume. The difference between the energy deposited and the energy released is accounted for by using an effective detector thickness which is based on the above estimated size of the dead layer.

When a monoenergetic beam of  $j$  particles of energy  $E' \text{ MeV}$  and unit flux  $\phi_j(0, E) = \delta(E - E')$  is incident upon a solid state detector, of effective thickness  $d \text{ g/cm}^2$ , the emerging flux is given by

$$\phi_j(d, E) = \frac{\exp\left\{-\frac{[E - E_j(d, E')]^2}{2s_j(d, E')^2}\right\}}{\sqrt{2\pi}s_j(d, E')}, \quad (8)$$

where  $E_j(d, E') = R_j^{-1}[R_j(E') - d]$  is the mean energy at depth  $d$ ,  $s_j(d, E')$  is the corresponding energy straggling width and  $R_j$  is the usual energy range function (Wilson et al., 2002).

Since a particle emerging with energy  $E$  has experienced an energy loss of  $E^d = E' - E$ , we can express the emerging flux as a function of energy loss as follows:

$$\phi_j(d, E) = f_j(d, E^d, E') = \frac{\exp\left\{-\frac{[E' - E_j(d, E') - E^d]^2}{2s_j(d, E')^2}\right\}}{\sqrt{2\pi}s_j(d, E')}. \quad (9)$$

The function  $f_j(d, E^d, E')$  so defined is called the unit spectral loss function.

When the incident flux of  $j$  particles is a more general function  $\phi_j(0, E) = \phi_j(E)$  the emerging flux is clearly given by

$$\phi_j(d, E) = F_j(d, E^d) = \int f_j(d, E^d, E') \phi_j(E') dE', \quad (10)$$

where, in general, computation of the spectral loss function  $F_j(d, E^d)$  requires numerical integration. However, in the special case where  $\phi_j(E)$  is a Gaussian function

$$\phi_j(E) = \frac{\exp\left\{-\frac{[E - E_0]^2}{2s_0^2}\right\}}{\sqrt{2\pi}s_0} \quad (11)$$

it is not difficult to show that

$$F_j(d, E^d) \approx \frac{\exp\left\{-\frac{[E_0 - E_j(d, E_0) - E^d]^2}{2s^2}\right\}}{\sqrt{2\pi}s}, \quad (12)$$

where

$$s = \sqrt{s_j(d, E_0)^2 + (r_0 s_0)^2}, \quad (13)$$

$$r_0 = 1 - \frac{S_j[E_j(d, E_0)]}{S_j[E_0]} \quad (14)$$

and  $S_j[E]$  is the change in  $E$  per unit distance.

In general, the flux of charged particles incident on the detector will consist of the fragment fluxes  $\{\phi_j(E)\}_{j=2}^k$ , in which case the energy loss spectrum  $F(d, E^d)$  is given by

$$F(d, E^d) = \sum_{j=2}^k F_j(d, E^d). \quad (15)$$

It should be noted that the ion index  $j = 1$  corresponds to the neutron flux that is not easily detected by the silicon detectors used in the present model.

### 3. The Experiments

Recently the Brookhaven National Laboratory Alternating Gradient Synchrotron (BNL AGS) was used to study fragmentation in several types and thicknesses of prospective shielding materials. Among the target materials used in this experiment were graphite-epoxy, and Aluminum. The beam ion was  $^{56}\text{Fe}$ , the heaviest ion present in significant numbers in the GCR. The energy at extraction from the AGS was 1087 MeV/nucleon and after passing through upstream beamline elements and detectors the beam energy at the entrance to the target was 1053 MeV/nucleon.

The detector configuration for this experiment was of the type shown schematically in Fig. 1. The experimental setup was similar to those for previous measurements by the same group (Miller et al., 1998,2003, Zeitlin et al., 1996,1997,1998,2001) using silicon detectors. The detectors upstream of the target were used to identify Fe beam particles by their energy deposition in the silicon. The three pairs of detectors downstream of the target were used to determine fragment charges and energies. They subtended angles of  $7.5^\circ$  (PSD2),  $2.5^\circ$  (d3mm1/2) and  $1.0^\circ$  (d3mm3/4) centered around the beam axis, as seen from a point at target-center. Data acquisition was initiated by an event trigger, defined as a coincidence of beam signals in detectors TR and d3mmU. The discriminator thresholds were set to accept as many Fe beam events as possible, and therefore some triggers were generated by fragments within a few charge units of Fe created by upstream nuclear interactions. These events were eliminated in the offline analysis, as were events where two or more Fe ions passed through the system close enough in time to be recorded in a single event.

For each event, the data acquisition system recorded energy deposition in each detector, position information from the two position-sensitive detectors (PSD1 and PSD2) and additional high gain energy deposition signals from each of the four downstream 3 mm-thick silicon detectors (d3mm1-4). The high gain signals were used to help identify the lightest charged fragments. Each PSD consisted of a pair of 1 mm-thick detectors measuring vertical and horizontal position in the plane normal to the beam axis. Each of these detectors

generated three signals: two position-dependent (“L” and “R” or “U” and “D”) and one total energy loss (“DEX” or “DEY”). For example, the output signals from the horizontal detector of PSD1 were DEX1, L1 and R1. The position-dependent signals can be used to obtain the particle coordinates normal to the beam, but in this analysis they were used only to select on particle energy loss. Data were also taken with no target in order to measure “background” production of fragments and losses of primaries, for example by interactions in the detectors and other materials along the beamline.

The analysis procedure was similar to that described in detail in previous publications (Miller et al., 1998,2003, Zeitlin et al., 1996,1997,1998,2001). Histograms and scatterplots were made of the energy deposition,  $\Delta E$ , in the detectors, and graphical cuts were used to select or reject events according to specific criteria. The first set of cuts, on detectors upstream of the target, required a single iron ion in both TR and d3mmU and correlated  $\Delta E$  signals consistent with an iron ion in the PSD1 detectors. For events satisfying these cuts, subsequent cuts selected events with either a surviving primary ion or one or more fragments. The sample of good events was defined by requiring correlated energy loss in the detectors of each pair. An additional set of cuts excluded events where a beam ion interacted in one of the detectors downstream of the target.

The detectors downstream of the target subtended small angles around the beam axis, and thus for most events recorded a single primary ion or a small number of fragments at or near the beam velocity. There are peaks in the  $\Delta E$  spectra corresponding in most cases to the individual fragment charges, as shown in figures 2-3. The number of fragments in each peak was determined by summing over the bins between valleys. Double Gaussian fits to adjacent peaks were used to allocate the relatively small number of counts in the regions where two peaks overlapped significantly.

#### 4. Results

In modeling the experiment described above, it was assumed that the  $^{56}\text{Fe}$  beam extracted from the AGS at 1087 MeV/nucleon was nearly monoenergetic (the small inherent energy width had no influence on subsequent comparisons). The Green's function solution was used to estimate the flux of the fragments entering the detector pair d3mm3 /d3mm4, which were treated as a single 6mm detector. The energy deposited by each fragment was then computed by means of Eqs. (9) and (10) and used to evaluate the energy loss spectrum as given by Eq. (15) using the NUCFRG2 nuclear database (Wilson et al., 1994b) and the QMSFRG nuclear data base (Cucinotta et al., 2003). Some results are exhibited in figures 2 through 3 where the computed energy loss spectrum (red curve) is compared with the experimental measurements (black curve), and in figure 4 where computations based on NUCFRG2 are compared with those based on QMSFRG.

The right hand peak is from the surviving ion beam and fragments produced by neutron removal. The next peak to the left is for Mn fragments followed by Cr fragments and so on. It appears that the Mn fragments are under represented by the NUCFRG2 model (Wilson et al., 1994b), which is consistent with earlier cross section measurements (Zeitlin et. al, 1997). Overall, the fragmentation cross sections in Al seem better represented by NUCFRG2 than those for the graphite-epoxy composite. Additionally, there was no appreciable difference between the NUCFRG2 results and the QMSFRG results for the Aluminum target. An additional discrepancy is the energy downshift parameter for large mass removal especially for vanadium and lighter fragments.

In order to further validate the model, it is desirable to compare with more than just the energy deposited in the detectors. It is advantageous to make comparisons with data that is derived from the fluences emerging from the target. The easiest of these to compare with is the track average LET,  $\langle \text{LET} \rangle_{\text{trk}}$ . The  $\langle \text{LET} \rangle_{\text{trk}}$  can be computed from the formula

$$\langle \text{LET} \rangle_{\text{TRK}} = \frac{\sum_i \int L_i(E) \frac{dN_i}{dE} dE}{\sum_i \int \frac{dN_i}{dE} dE} \quad (16)$$

where  $\frac{dN_i}{dE}$  is the flux and  $L_i(E)$  is the LET of the  $i^{\text{th}}$  particle type at energy  $E$ . In order to be able to make comparisons with experimental data, we will take  $L_i(E)$  to be  $LET_{\infty}$  in water for particle  $i$  at energy  $E$ ; i.e., the stopping power,  $S_i(E)$ , for water.

The light ions,  $Z = 1, 2$  have a strong angular dependence and, as a consequence of the straightahead approximation, there is a marked over prediction in their fluences. If uncorrected, the predictions for the  $\langle \text{LET} \rangle_{\text{trk}}$  would be drastically lower than experiments, due to the artificial inflation of the denominator in Eq. (16). It is possible to correct for this by scaling  $\frac{dN_i}{dE}$  by an appropriate weight factor for each of the light ions, thereby

reducing their number and dampening effect. The weight factors are 0.02 for  $Z = 1$  and 0.08 for  $Z = 2$ . These corrections are used for all targets.

Table 1 shows  $\langle \text{LET} \rangle_{\text{trk}}$  computed from the model with the corrected fluences and preliminary results from experiments done at Brookhaven National Laboratory Alternating Gradient Synchrotron (BNL AGS) for various targets and thickness. All of the experiments were carried out with a 1 GeV/amu  $^{56}\text{Fe}$  beam. In all cases, there is reasonable agreement between the predictions of the model and the experimental results with the greatest error occurring in the Graphite-Epoxy results.

## 5. Concluding remarks

The computed spectrum exhibited in figures 2 and 3 has the right general shape and, for the most part, is in reasonable agreement with the experimental results. Discrepancies, particularly at the lower values of deposited energy, indicate a need for model refinement and further comparison with experimental measurement. In consequence, the light ion component of the model is currently under revision and an effort is being made to incorporate the effects of multiple scattering and the off-axis production components of ion fragmentation.

## References

Cucinotta, F. A., Saganti, P. B., Hu, X., et al., Physics of the Isotopic Dependence of Galactic Cosmic Ray Fluence Behind Shielding. NASA/TP-2003-210792, Feb. 2003.

Miller, J., Laboratory Validation of Material Shielding Properties, in: Wilson, J. W., Miller, J., and Cucinotta, F. A. (Eds.), Shielding Strategies for Human Space Exploration, NASA/CP-3360, pp. 427-433, 1998.

Miller, J., Zeitlin, C., Cucinotta, F. A., et al., Benchmark studies of the effectiveness of structural and internal materials as radiation shielding for the international space station, Rad. Res, 159,381-390,2003.

Tripathi, R. K., Townsend, L. W., Kahn, F., Role of intrinsic width in fragment momentum distributions in heavy ion collisions, Phys. Rev. C., 48(4), R1775-R1777, 1994.

Tweed, J., Wilson, J. W., Tripathi, R. K., An improved Green's function for ion beam, Advances in Space Research, (to appear), 2004.

Wilson, J. W., Analysis of the theory of high-energy ion transport. . NASA TN D-8381,1977.

Wilson, J. W., Lamkin, S. L., Farhat, H., et. al., A closed form solution to HZE propagation , Radiat. Res., 122, 223-228, 1990.

Wilson, J. W., Townsend, L. W., Schimmerling, W., et al., Transport Methods and Interactions for Space Radiations, NASA RP-1257, 1991.

Wilson, J. W., Shavers, M. R., Badavi, F. F., et al., Nonperturbative Methods in HZE Propagation, Radiat. Res., 140, 241-248, 1994a.

Wilson, J. W., Shinn, J. L., Townsend, L. W., et al., NUCFRG2: A semi-empirical nuclear fragmentation model. Nucl Inst. Methods Phys. Res. B 94, 95, 1994b.

Wilson, J. W., Tweed, J., Tai, H., et al., A simple model for straggling evaluation, Nucl. Instr. and Meth. in Phys. Res. B 194, 389-392, 2002.

Zeitlin, C., Miller, J., Heilbronn, L. H., et al., The fragmentation of 510 MeV/nucleon iron-56 in polyethylene. I. Fragment fluence spectra. Rad. Res. 145, 655-665 ,1996.

Zeitlin, C., Heilbronn, L. H., Miller, J., et al., Heavy fragment production cross sections from 1.05 GeV/nucleon  $^{56}\text{Fe}$  C, Al, Cu, Pb and CH<sub>2</sub> targets. Phys. Rev. C 56, 388-397, 1997.

Zeitlin, C., Heilbronn, L. H., Miller, J., Detailed characterization of the 1087 MeV/nucleon  $^{56}\text{Fe}$  beam used for radiobiology at the AGS. Radiat. Res. 149, 560-569, 1998.

Zeitlin, C., Fukumura, A., Heilbronn, et al., Fragmentation Cross Sections of 600 MeV/nucleon  $^{20}\text{Ne}$  on Elemental Targets. Phys. Rev. C 64, 024902, 2001.

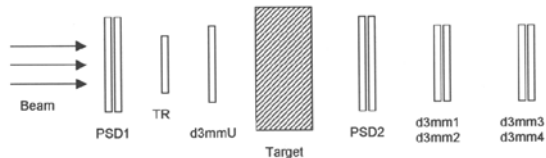


FIG. 1. Detector configuration (not to scale). All detectors are silicon; the trigger detector TR detector effectively defines the size of the usable beam spot. The respective thicknesses and approximate active areas are: TR – 300  $\mu\text{m}$  x 300  $\text{mm}^2$ ; PSD1 and PSD2 – 1  $\text{mm}$  x 1500  $\text{mm}^2$ ; d3mmU and d3mm1-4 – 3  $\text{mm}$  x 450  $\text{mm}^2$ .

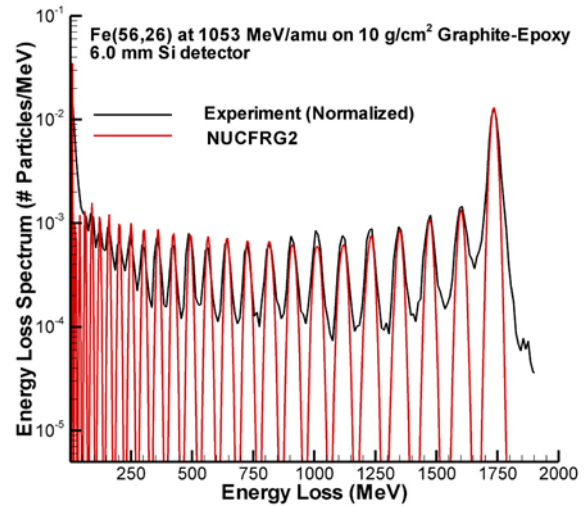


FIG 2: Summed energy loss (MeV) in the detector pair d3mm3/4 for fragments produced by 1053 MeV/nucleon  $^{56}\text{Fe}$  ions in 10  $\text{gm}/\text{cm}^2$  graphite-epoxy (50.92/49.08%).

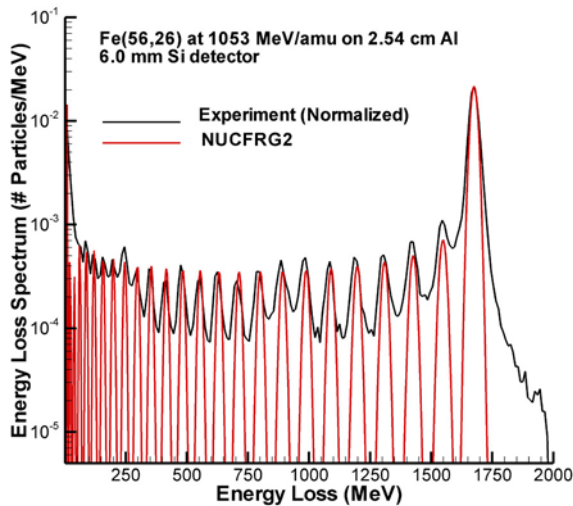


FIG 3: Summed energy loss (MeV) in the detector pair d3mm3/4 for fragments produced by 1053 MeV/nucleon  $^{56}\text{Fe}$  ions in 2.54 cm Al.

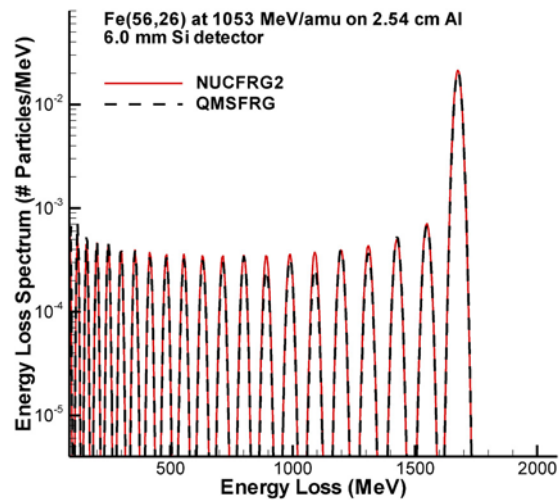


FIG 4: The summed energy loss (MeV) in the detector pair d3mm3/4 for fragments produced by 1053 MeV/nucleon  $^{56}\text{Fe}$  ions in 2.54 cm Al, as predicted by computations based on NUCFRG2 and QMSFRG

Material	Depth (g/cm <sup>2</sup> )	$\langle \text{LET} \rangle_{\text{trk}}$ model	$\langle \text{LET} \rangle_{\text{trk}}$ experiments
Carbon	3.9	125.3	127.0
Aluminum	7	127.3	125.4
Lead	3.6	148.2	145.8
Polyethylene	10	91.3	91.4
Graphite-Epoxy	5	116.3	121.3
Graphite-Epoxy	10	94.8	98.5

TABLE 1: Track Averaged LET from Model and Experiments. Angular factor for z=1 (2) is 0.02 (0.08)